CSCE Annual Conference

Growing with youth – Croître avec les jeunes

Laval (Greater Montreal)

June 12 - 15, 2019

Determination of Critical Elastic Buckling Loads and Half-wavelengths of Rack Columns with Patterned Perforations

Peng Zhang[1,2], M. Shahria Alam[1,3]

[1] The University of British Columbia, Canada
[2] p.zhang@alumni.ubc.ca
[3] shahria.alam@ubc.ca

Abstract: Currently, rack columns with Σ-shaped sections and patterned perforations are often used to form upright frames of storage pallet racks. These rack columns are subjected to buckling failure under compression. Analytical design solutions (e.g., the Direct Strength Method in AISI_S100 (2016)) have been proposed by scientists for designing perforated rack columns under compression. The critical elastic buckling loads of rack columns are usually the input parameters of analytical design solutions, and the critical elastic buckling half-wavelengths provide references for predicting their buckling modes. As a result, the determination of critical elastic buckling loads and half-wavelengths is critical while these parameters now can only be estimated by using approximate or simplified methodologies (e.g., effective thickness method). In this paper, rack columns with three different Σ-shaped sections and patterned perforations are investigated. The material properties of the columns are experimentally determined. The stress-strain curves present a significant yield plateau; hence, an expanded Ramberg-Osgood model is proposed for describing the curves with high accuracy. The multi half-wavelengths method is proposed by using which the critical elastic buckling loads and half-wavelengths of the rack columns are determined accurately.

1 INTRODUCTION

Rack columns are generally cold-formed from thin-walled steel sheets, and patterned perforations are often punched in the columns along the length uniformly. The columns are used to form upright frames of storage pallet racks. An example of storage pallet racks is presented in Figure 1, and their structural members are shown in Figure 2.

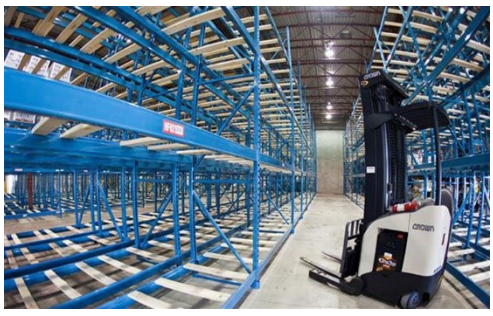

Figure 1: Storage pallet racks (Zhang and Alam 2017)

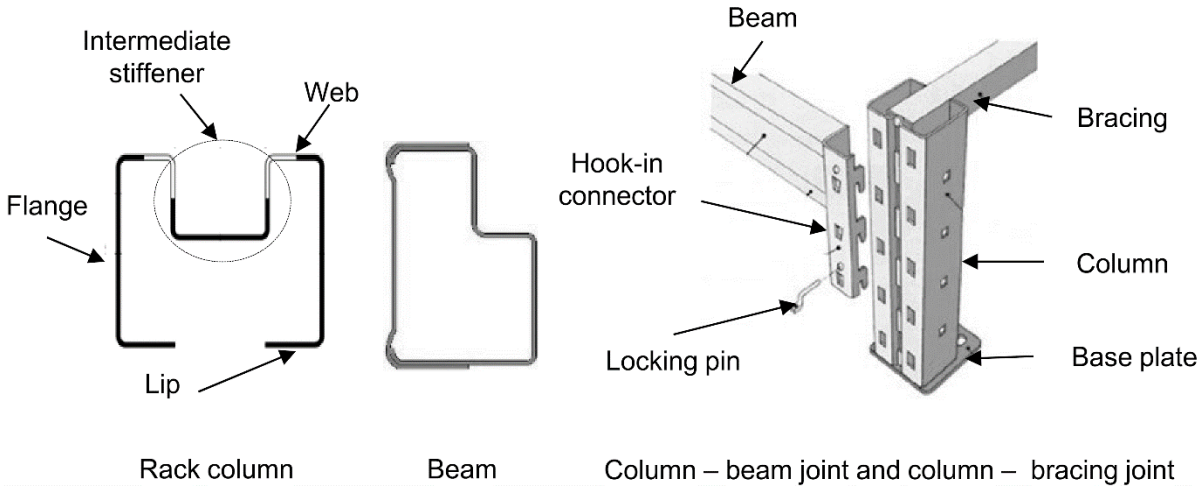

Figure 2: Structural members of storage pallet racks

The beam-column joints of pallet racks are generally the mechanical interlock connections; see Figure 2. Holes in rack columns make the assembly of the connections becomes easy and flexible. Traditional rack columns usually have a plain channel or lipped channel section, and very few perforations are made at beam-column or column-bracing joints for making bolted connections. Nowadays, rack columns with a complex shape of section (e.g., Σ or Ω section) have gained great popularity in North America. These sections are open and singly symmetric, which impose great difficulties on engineers for designing the columns analytically. The first reason is that multiple buckling modes need to be considered for rack columns in design. The common buckling modes of Local (L), Distortional (D), Torsional + Flexural (TF), and Flexural (F) of a rack section are shown in Figure 3. TF and F are usually jointly termed as Global (G) buckling mode. The definitions of these buckling modes are given in the AISI_S100 (2016). Different buckling modes may present on a rack column simultaneously, and the column presents an interactive buckling mode, e.g., L + D, L + G, and D + G (Casafont et al. 2011; Dinis et al. 2014; Kwon et al. 2009; Yang and Hancock 2004). The second reason is that perforations affect the critical elastic buckling loads and half-wavelengths of rack columns significantly while the computer programs of the CUFSM v4.05 (Li and Schafer 2010) and GBTUL 2.0 (Bebiano et al. 2018) cannot handle perforations in their numerical models. These two computer programs are user-friendly and are generally employed by engineers and scientists for determining elastic buckling properties of rack columns without perforations.

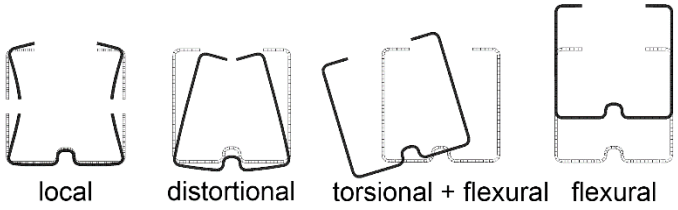

Figure 3: Cross-sectional deformation of different buckling modes

The study of the buckling behaviour of rack columns under compression can be traced back to 1980s. The distortional buckling behaviour of rack columns under compression was firstly investigated by Hancock (1985). Hancock and Roos (1986) experimentally studied the TF buckling behaviour of two rack columns without perforations. The rack columns were assembled in a single span of upright frame and were compressed axially till failure. The buckling behaviour of two different types of perforated rack columns under compression was experimentally studied by Davies et al. (1997). The effective thickness method was proposed for considering the perforations, which was employed with the Generalized Beam Theory (GBT) to predict the compression capacity of the columns. Yang and Hancock (2004) physically tested solid and high-strength rack columns under compression. The columns presented L + D buckling, and their ultimate loads varied significantly with the collapsed shape of the columns. The buckling behaviour of perforated

rack columns under compression was experimentally studied by Casafont et al. (2011). It was observed that distortional buckling modes always accompanied by a global buckling mode in the columns. Casafont et al. (2012) experimentally evaluated the accuracy of the Direct Strength Method (DSM) (*AISI_S100* 2007) for predicting the capacity of perforated rack columns under compression. Dinis et al. (2014) experimentally investigated the L + D buckling behaviour of rack columns without perforations. Yao and Rasmussen (2016) proposed an analytical design solution (Proposed Method 2), which was claimed to be capable of designing perforated thin-walled columns with multiple different shapes of cross-sections. Zhao et al. (2017) performed a large number of compression tests on rack columns with and without perforations. Rack columns with four different sections and various lengths were tested so that their buckling behaviour of D, D + G, and G were investigated. The local buckling behaviour of perforated rack columns with three different Σ-shaped sections was investigated by Zhang and Alam (2017), and these three rack sections are investigated in this paper.

From the literature review, it can be concluded that it is necessary to propose an accurate and unbiased method for determining the critical buckling loads and half-wavelengths of rack columns with perforations. This problem is addressed in this paper. Additionally, stress-strain curves with a significant yield plateau are presented in material property tests; hence, an analytical model named as expanded Ramberg-Osgood model is proposed here for describing these curves accurately.

2 Rack Columns

2.1 Rack column profiles

Rack columns with three different Σ-shaped sections produced in North America were selected for this study. The nominal net cross-sections and the column profiles are shown in Figure 4. The net cross-section of a rack column with perforations is the cross-section that has the minimum area along the length. The dimensions of the nominal cross-sections are shown in Table 1, and they were measured along the outer face of cross-sections while the corner radii were measured along the middle face of the cross-sections. The rack columns have the same thickness of 1.80mm; all the corners of the cross-sections are right angles.

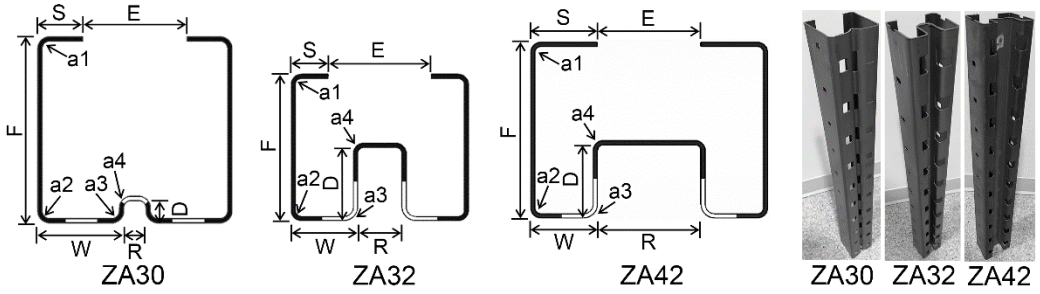

(a) nominal net cross-sections (b) rack column profiles

Figure 4: Nominal cross-sections and column profiles

Table 1: Dimensions of column nominal cross-sections

Column	Dimension (mm)						Radius (mm)				Area (mm^2)	
	S	F	W	R	D	E	a1	a2	a3	a4	A_{net}	A_{gross}
ZA30	19.05	79.38	36.51	9.53	9.53	44.45	4.08				432.75	499.97
ZA32	19.05	63.50	28.58	19.05	31.8	38.10	3.44	3.44	4.96	3.44	408.53	512.06
ZA42	28.58	76.20	28.58	44.45	31.8	44.45	3.44	3.44	4.97	3.44	534.26	637.78

2.2 Material properties

Material properties of the rack columns are experimentally determined, and the results are presented in Table 2. The details about the tests can be found in (Zhang and Alam 2017).

Table 2: Material Properties

Section	Engineering properties					
	E ($\times 10^5\ MPa$)	LYS (MPa)	UYS (MPa)	F_u (MPa)	ε_{F_u} (%)	ε_f (%)
ZA30	2.06	473	480	571	12.9	19.5
ZA32	2.08	466	476	564	12.2	18.8
ZA42	2.06	468	472	569	13.0	21.5

Note: E =Young's modulus, LYS = Lower yield strength, UYS = Upper yield strength, F_u = Tensile strength, ε_{F_u} = Strain at F_u, ε_f = Fractural strain.

3 Expanded Ramberg-Osgood model

An expanded Ramberg-Osgood (R-O) model is proposed for describing stress-strain curves with a yield plateau; see Equation 1 and Figure 5. The detailed information of this model can be found in (Zhang and Alam 2017). The experimentally determined stress-strain curves are shown in Figure 6.

$$[1]\varepsilon = \begin{cases} {}^{\sigma}/_{E}, & 0 \le \sigma \le \sigma_e \\ \sigma/E + k_1(\sigma/E)^{n_1}, & \sigma_e < \sigma \le f_y \\ \varepsilon_y + (\sigma - f_y)/\alpha E, & f_y < \sigma \le \sigma_p \\ \sigma/E + k_2(\sigma/E)^{n_2}, & \sigma > \sigma_p \end{cases}$$

where

σ – true stress

σ_e –the proportional limit is the point, where the relative difference between the R-O stress, (from $\varepsilon = \sigma/E + k_1(\sigma/E)^{n_1}$), and the linear stress ($\sigma = \varepsilon E$) is larger than 0% but less than or equal to 0.5% (Equation 2), is chosen as the proportional limit.

ε – true strain

E – Young's modulus

f_y – yield strength. Here, the lower yield strength is defined as f_y.

ε_y – the strain at f_y.

n_1, n_2, k_1, k_2 – constants, they are calculated according to Equations 3, 4, 5, and 6, respectively.

α – a coefficient multiplied with E represents the slope of the yielding platform. It is determined through linear fittings of yielding platforms. Yielding platform starts from ε_y to the points where tangent moduli starts to change stably (has no negative sign and without significant variations). It can be determined graphically by plotting the tangent moduli against strains of that portion.

ε_p – the strain at the intersection of a yielding platform and initial strain hardening portion.

σ_p – the stress at ε_p.

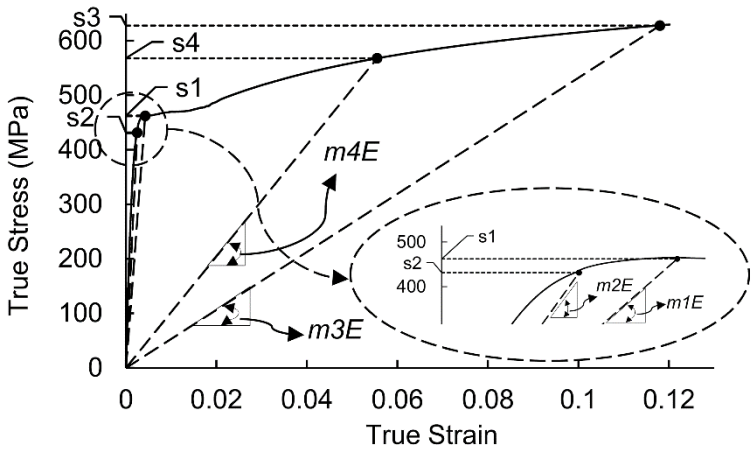

Figure 5: Determination of secant yield strength

$$[2]0 < \frac{|\sigma_e - \varepsilon E|}{\sigma_e} \leq 0.5\%$$

$$[3]n_1 = 1 + \frac{\log\frac{m_2(1-m_1)}{m_1(1-m_2)}}{\log\left(\frac{s_1}{s_2}\right)}$$

$$[4]n_2 = 1 + \frac{\log\frac{m_4(1-m_3)}{m_3(1-m_4)}}{\log\left(\frac{s_3}{s_4}\right)}$$

$$[5]k_1 = (1/m_2 - 1)(s_2/E)^{1-n_1}$$

$$[6]k_2 = (1/m_4 - 1)(s_4/E)^{1-n_2}$$

where s_1, s_2, s_3 and s_4 are secant yield strengths. They are equal to the ordinates of the intersections with the stress-strain curve of lines through the origin having the slopes equal to m_1E, m_2E, m_3E, and m_4E, respectively. An example is presented in Figure 5 for an illustration. m_1 and m_2 are determined by Equations 7 and 8 where, m_3 and m_4 are being chosen where the intersections are close to the ultimate stress and the center of the strain hardening portion, respectively.

$$[7]m_1 = f_y/\left(f_y + 0.002E\right)$$

$$[8]m_2 = 0.85$$

Six engineering stress-strain curves obtained through standard material tensile tests are used for the model validation. The engineering stress and strain are converted to true stress and true strain by using Equations 9 and 10, respectively. The stress-strain data after ultimate engineering stress were discarded because necking probably occurred from here. The results show that when strain is beyond the proportional limit, errors are less than 5%, which proved the effectiveness of the model. Three stress-strain curves were generated by using the expanded R-O model, and they are plotted together with the corresponding true stress-strain curves in Figure 6.

$$[9]\sigma = \sigma_{eng}\left(1 + \varepsilon_{eng}\right)$$

$[10]\varepsilon = ln(1 + \varepsilon_{eng})$ where σ_{eng} – engineering stress and ε_{eng} – engineering strain.

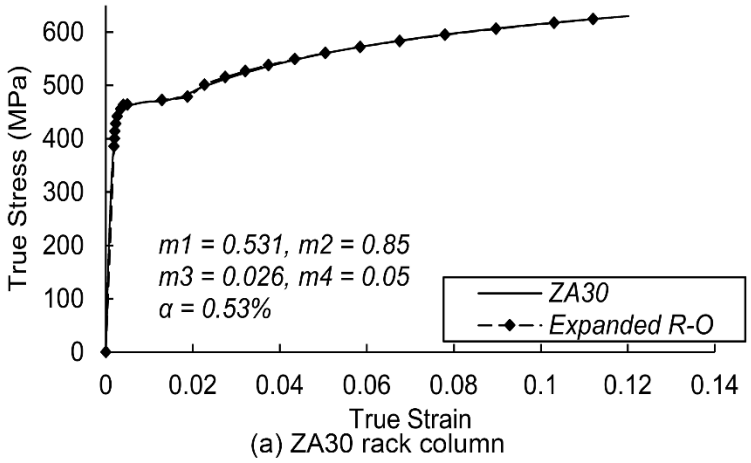

(a) ZA30 rack column

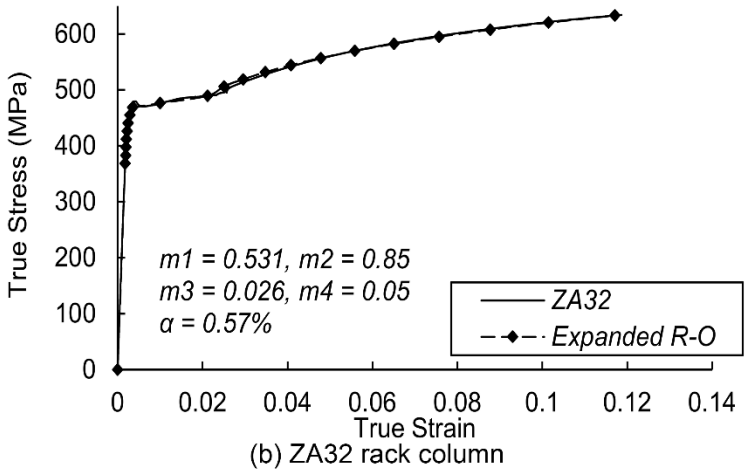

(b) ZA32 rack column

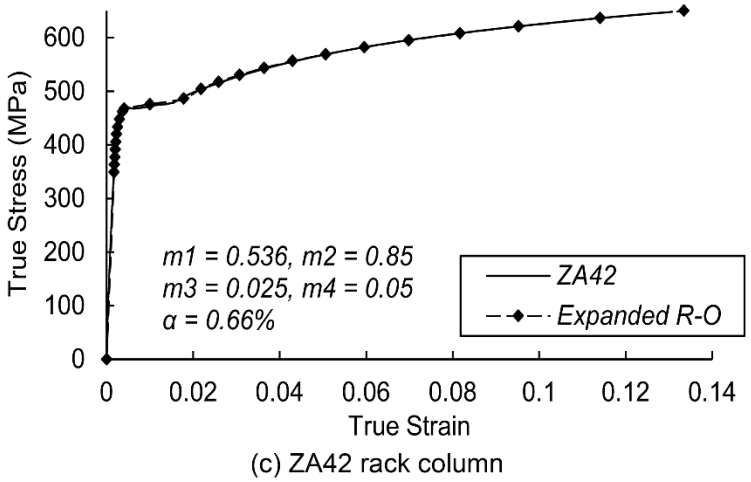

(c) ZA42 rack column

Figure 6: Strain-stress curves

4 Multi-half-wavelengths method

Hancock (1985) pointed out that when a rack column presents multiple local (or distortional) half-wavelengths, the end boundary conditions will have very little effect on its buckling load. This phenomenon is termed here as the multi-half-wavelengths effect. It is assumed here that for a rack column with the length of mL and under Clamped-Clamped (C-C) boundary condition, when the m is large enough, its local (or distortional) buckling load converges to the local (or distortional) buckling load of the column with the length of L but under Simply-Simply (S-S) boundary condition. This assumption provides a way to determine the elastic buckling load (under the S-S boundary condition) of a perforated rack column with a specific half-wavelength. The m is the number of buckling half-wavelengths; the L is the half-wavelength. For the S-S boundary condition, the transversal displacements of column ends are restrained while the column ends are free to warp. For the C-C boundary condition, column ends are fixed except one of the ends (the loading end) can move longitudinally in the form of rigid-body movements. The critical half-wavelengths and buckling loads of a column are symbolized as $(l_{crl}^{S-S}, P_{crl}^{S-S})$, $(l_{crd}^{S-S}, P_{crd}^{S-S})$. The subscript of these symbols indicates the buckling mode: l is local buckling and d is distortional buckling. The superscript of these symbols indicates the boundary condition.

4.1 Numerical models

ANSYS 18.1 is used for numerically simulating the rack columns. The details about the modelling process can be found in (Zhang and Alam 2019). Eigenbuckling analyses are performed on the rack columns under the C-C boundary condition, and the models have the length of ml and are braced at the ends of each buckling half-wavelength. An example of a numerical model of the ZA32 section is presented in Figure 7. Few nodes at the cross-sections of $Z = nL$ $(n = 1, 2, 3, \ldots m-1)$ are selected for the three rack sections; see Figure 8. The bracing is achieved by restraining the out-of-plane displacement of these nodes. By doing this, fixed buckling half-wavelengths can be defined, and the interactions of local or distortional buckling with higher order buckling modes are prevented. The results of the sensitivity analysis show that when $m = 11$, the effect of the boundary condition can be almost fully diminished. Eigenbuckling analyses are performed by gradually changing the L; hence, a buckling curve can be generated. The minimum point in the buckling curve shows the critical buckling half-wavelength and critical buckling load.

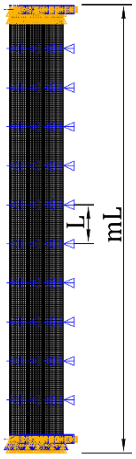

Figure 7: A numerical model of ZA32 rack column

4.2 Validation of the method

The multi-half-wavelengths method is applied to the three rack sections without considering the perforations. The yielded bucking curves are presented in Figure 9. The buckling curve of the ZA42 section failed to distinctly show the $(l_{crd}^{S-S}, P_{crd}^{S-S})$; consequently, it was determined by using the methodology of $FSM@cFSM - l_{cr}$ (Li and Schafer 2010). The same phenomenon was observed from the buckling curve yielded from the CUFSM v4.05 (Li and Schafer 2010). The results of $(l_{crl}^{S-S}, P_{crl}^{S-S})$ and $(l_{crd}^{S-S}, P_{crd}^{S-S})$ of the rack

sections determined here are compared with the results yielded from the CUFSM v4.05 (Li and Schafer 2010); see Table 3. The comparison shows that the differences between the results yielded by the two methods are less than 2%. The multi-half-wavelengths method is successfully validated here.

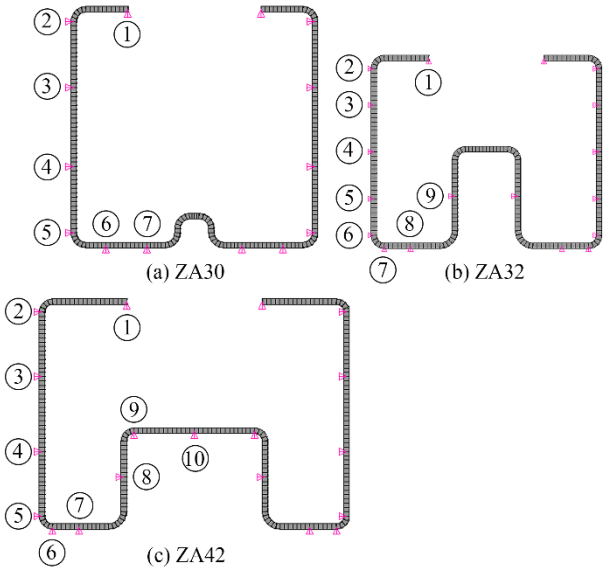

Figure 8: The selected nodes restrained at the cross-sections

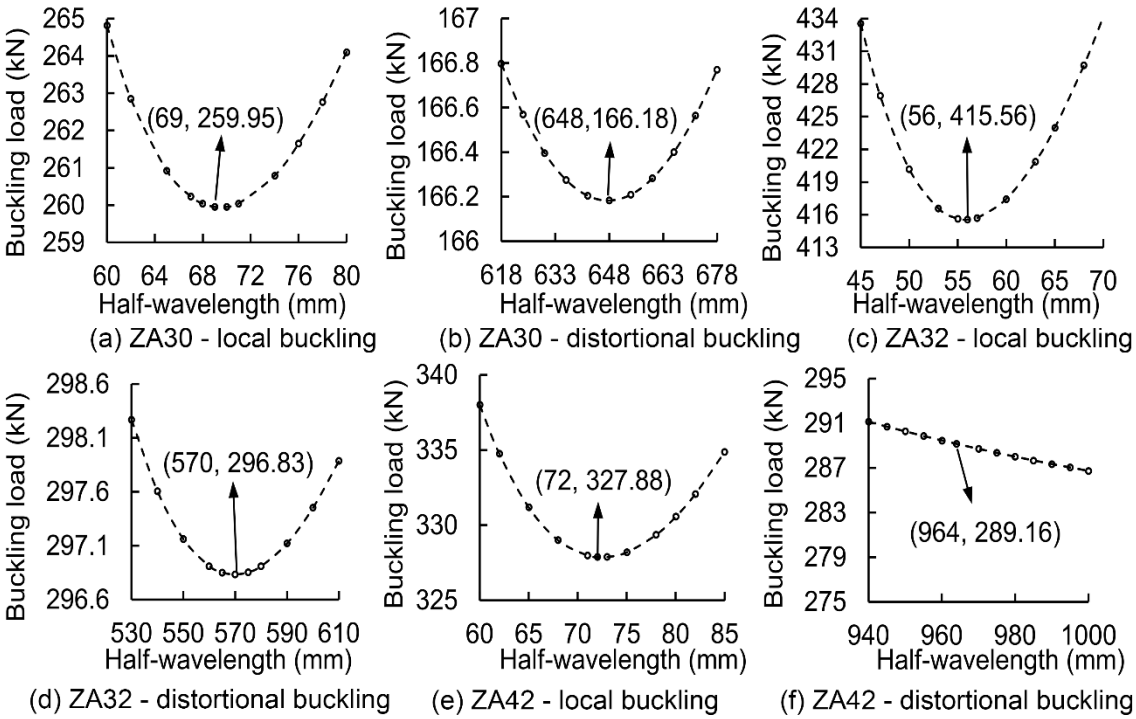

Figure 9: Buckling curves of the three rack sections

4.3 Determination of $(l_{crl}^{S-S}, P_{crl}^{S-S})$ and $(l_{crd}^{S-S}, P_{crd}^{S-S})$ of perforated rack sections

The multi-half-wavelengths method is applied to determine the $(l_{crl}^{S-S}, P_{crl}^{S-S})$ and $(l_{crd}^{S-S}, P_{crd}^{S-S})$ of the three rack sections with perforations, and the perforation pattern effects are considered. The results are presented in Figure 10. The details of the perforation pattern effects are described in (Zhang and Alam 2019).

Table 3: Critical elastic buckling loads and half-wavelengths of sold rack sections

Section	CUFSM				Multi-half-wavelengths method			
	P_{crl}	l_{crl}	P_{crd}	l_{crd}	P_{crl}	l_{crl}	P_{crd}	l_{crd}
ZA30	259.8	69.0	164.9	641.0	260.0	69.0	166.2	648.0
ZA32	415.0	55.0	292.8	563.0	415.6	56.0	296.8	570.0
ZA42	325.6	71.0	284.2	964.0*	327.9	72.0	289.2	964.0*

Note: * means the parameter is determined by using the methodology of $FSM@cFSM - l_{cr}$.

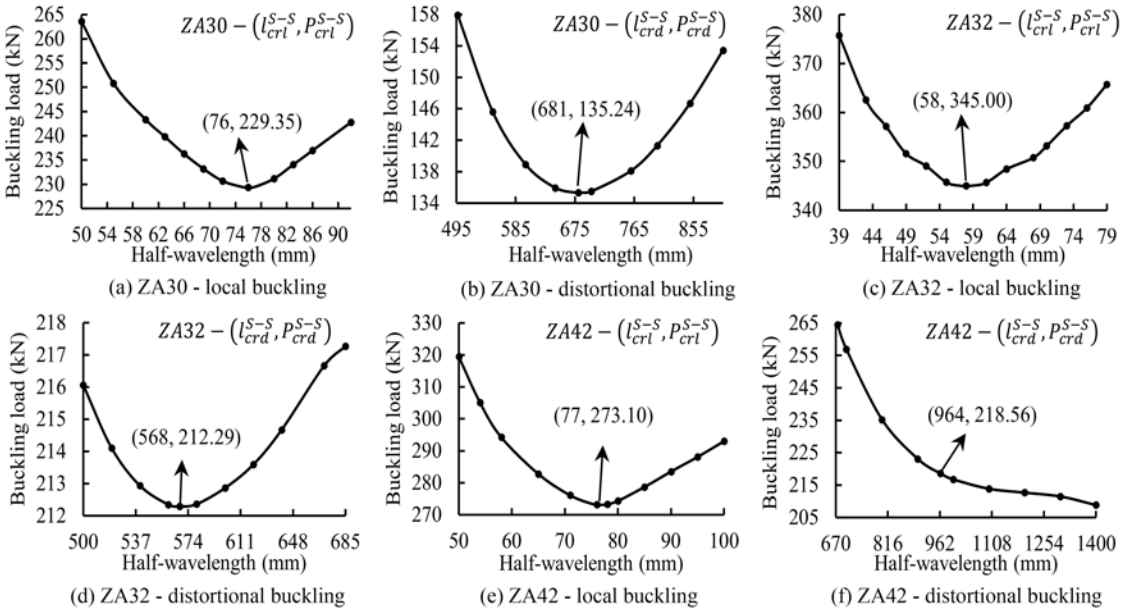

Figure 10: Buckling curves of the three rack sections with perforations

5 Conclusion

This paper introduced the expanded Ramberg-Osgood model, which can be used for accurately describing stress-strain curves with a significant yield plateau. The multi half-wavelengths method is introduced as well by using which the critical elastic buckling loads and half-wavelengths of the rack sections with and without perforations can be accurately determined.

6 Acknowledgements

Financial contributions of Natural Sciences and Engineering Research Council of Canada (NSERC) [Engage Grant], College of Graduate Studies of University of British Columbia [University Graduate Fellowship], and China Scholarship Council [CSC scholarship] were critical to conduct this study. The authors also acknowledge CMC Microsystems for the provision of products and services that facilitated this research, including ANSYS Multiphysics.

7 References

AISI_S100 (2007). "North American Specification for the Design of Cold-Formed Steel Structural members." American Iron and Steel Institute, Washington, DC.

AISI_S100 (2016). "North American Specification for the Design of Cold-Formed Steel Structural members." American Iron and Steel Institute, Washington, DC.

Bebiano, R., Camotim, D., and Gonçalves, R. (2018). "GBTul 2.0− A second-generation code for the GBT-based buckling and vibration analysis of thin-walled members." *Thin Wall Struct.*, 124, 235-257.

Casafont, M., Pastor, M. M., Roure, F., Bonada, J., and Peköz, T. (2012). "Design of steel storage rack columns via the direct strength method." J Struct Eng., 10.1061/(ASCE)ST.1943-541X.0000620/669-679.

Casafont, M., Pastor, M. M., Roure, F., and Peköz, T. (2011). "An experimental investigation of distortional buckling of steel storage rack columns." Thin Wall Struct., 49(8), 933-946.

Davies, J. M., Leach, P., and Taylor, A. (1997). "The design of perforated cold-formed steel sections subject to axial load and bending." Thin Wall Struct., 29(1), 141-157.

Dinis, P. B., Young, B., and Camotim, D. (2014). "Local–distortional interaction in cold-formed steel rack-section columns." Thin Wall Struct., 81, 185-194.

Hancock, G. J. (1985). "Distortional Buckling of Steel Storage Rack Columns." J Struct Eng., 111(12), 10.1061/(ASCE)0733-9445(1985)111:12(2770).

Hancock, G. J., and Roos, O. (1986). "Flexural-torsional buckling of storage rack columns." Proc., *8th Int. Spec. Conf. on Cold-Formed Steel Structures*, W.-W. Yu, and J. H. Senne, eds. Department of Civil Engineering University of Missouri - Rolla, St. Louis, Missouri, US, 329-351.

Kwon, Y. B., Kim, B. S., and Hancock, G. J. (2009). "Compression tests of high strength cold-formed steel channels with buckling interaction." J Constr Steel Res., 65(2), 278-289.

Li, Z., and Schafer, B. (2010). "Application of the finite strip method in cold-formed steel member design." J Constr Steel Res., 66(8), 971-980.

Li, Z., and Schafer, B. "Buckling analysis of cold-formed steel members with general boundary conditions using CUFSM: conventional and constrained finite strip methods." Proc., *20th Int. Spec. Conf. on Cold-Formed Steel Structures*, R. A. LaBoube, and W.-W. Yu, eds. Missouri University of Science and Technology, St. Louis, Missouri, US.

Yang, D., and Hancock, G. J. (2004). "Compression tests of high strength steel channel columns with interaction between local and distortional buckling." J Struct Eng., 10.1061/(ASCE)0733-9445(2004)130:12(1954)/1954-1963.

Yao, Z., and Rasmussen, K. J. (2016). "Perforated Cold-Formed Steel Members in Compression. II: Design." J Struct Eng., 10.1061/(ASCE)ST.1943-541X.0001636/04016227.

Zhang, P., and Alam, M. S. (2017). "Experimental investigation and numerical simulation of pallet-rack stub columns under compression load." J Constr Steel Res., 133, 282-299.

Zhang, P., and Alam, M. S. (2019). "Elastic Buckling Behaviour of Σ-Shaped Rack Columns under Uniaxial Compression." *submitted to the Journal of ENG STRUCT.*, University of British Columbia, Kelowna, Canada.

Zhao, X., Ren, C., and Qin, R. (2017). "An experimental investigation into perforated and non-perforated steel storage rack uprights." *Thin Wall Struct.*, 112, 159-172.